Controlled modification of skyrmions information in a three-terminal racetrack memory

Journal:	*Nanoscale*
Manuscript ID	NR-ART-01-2019-000909.R1
Article Type:	Paper
Date Submitted by the Author:	05-Mar-2019
Complete List of Authors:	Wang, Kang; Nanjing University Qian, Lijuan; Brown University Ying, See-chen; Brown University Gang, Xiao; Brown University Wu, Xiaoshan; Nanjing University, NLSSMS

SCHOLARONE™
Manuscripts

Controlled modification of skyrmions information in a three-terminal racetrack memory

Kang Wang,[a,b] Lijuan Qian,[b] See-Chen Ying,[b] Gang Xiao,*[b] Xiaoshan Wu*[a]

[a]*Collaborative Innovation Center of Advanced Microstructures, Laboratory of Solid State Microstructures, School of Physics, Nanjing University, Nanjing 210093, China.* E-mail: xswu@nju.edu.cn

[b]*Department of Physics, Brown University, Providence, Rhode Island 02912, USA.* E-mail: gang_xiao@brown.edu

Abstract

Manipulation of magnetic skyrmions has been arousing considerable interest because of its potential applications in future spintronic devices. As an information carrier, a skyrmion is used to code a bit. In this work, we study via micromagnetic simulations a three-terminal racetrack memory, where an isolated skyrmion can be generated and annihilated by the gate voltage pulse. Thus, we can modify a train of skyrmion codes written at the generator in a controlled manner. The modified information is then detected at the collector. We have identified both gyration and breathing modes during skyrmion manipulation. The dynamics is analysed via a Thiele equation derived from the micromagnetic model. From the equation, the gyration mode of a skyrmion is suggested to be coupled to the breathing mode dynamics. This work proposes an effective method for controlled modification of skyrmion information in potential energy-efficient racetrack memories, and provides a fundamental understanding of the intrinsic skyrmion dynamics during skyrmion manipulation.

1   Introduction

Magnetic skyrmions are spin textures topologically stabilized in materials with various interactions including exchange, dipolar, anisotropy energy and an additional Dzyaloshinskii-Moriya interaction (DMI).[1-12] In particular, skyrmions observed in multilayers composed of a ferromagnetic layer and a heavy metal layer with strong spin-orbit coupling (SOC) have been receiving great interest.[4-10, 12] Interfacial DMI generated by SOC and broken inversion symmetry promises the stabilization of Néel-textured skyrmions (Fig. 1(a)) at the interface. The skyrmions can be driven by extremely low spin-polarized current,[8, 13] even at room-temperature and without external magnetic field.[9, 14] Most recently, a broad range of experimental and theoretical studies deal with skyrmions manipulation via controlling diverse parameters such as anisotropic constant and DMI.[12, 15-17] These operations on nano-sized skyrmions provide fundamental basis for potential skyrmion applications in the next generation of spintronic data storage and logical devices.[15, 18-24]

Similar to domain wall-based racetrack memory, a bit is coded by a skyrmion in a skyrmion-based magnetic storage memory. It has been proposed and demonstrated that a single skyrmion can be generated via a constricted structure,[9, 25] defects with lower magnetic anisotropy,[26, 27] or localized spin-orbit torque (SOT).[4, 13] The magnetization flips first in a defined region with larger SOT and then become stabilized by DMI. Annihilation of a skyrmion is generally achieved by driving it towards the boundary of a track,[13] or by employing a localized SOT to overcome the energy barrier between stable skyrmion and ferromagnetic states.[4] In addition to writing and deleting skyrmions, it is also essential to modify a train of skyrmion codes in a controlled manner. Arbitrary modification still remains a challenge so far. Various concepts have been proposed and realized recently, such as using the local spin-polarized current in scanning tunnelling microscopes [4] or a nanocontact geometry.[28] However, these models are hard to incorporate in actual devices. This inspires us to explore a new configuration for controlled modifications of a train of skyrmion codes in magnetic nanoribbons, as well as studying the intrinsic skyrmion dynamics in this geometry.

Skyrmion dynamics, including trajectories of the centre of mass and breathing modes (oscillatory variation of the skyrmion radius), are of increasing interest for both fundamental and technological reasons.[5, 29-33] The trajectories illustrate the nature of the skyrmion motion. In addition, it allows us to determine the value of the skyrmion inertial mass.[29] Gigahertz gyration eigenmode dynamics observed in the magnetic disk, as well as skyrmions motion in a nanoribbon,[5] can be well described by the Thiele equation when the inertial mass term is included.[5, 29] Besides gyration modes, breathing modes have also been observed for stable [30, 33] and even dynamically stabilized skyrmions.[32] Breathing mode frequency is also in the gigahertz region, which depends greatly on the spin current [31] and coupling between surrounding spin textures, such as adjacent topological bubbles.[33] The breathing mode also has an effect on skyrmion motion in the racetrack memory.[31] Thus, understanding of these modes provides insight into skyrmion manipulation. Descriptions of gyration and breathing modes that consider both SOT and boundary effects have so far remained elusive. The correlation between gyration and breathing modes also remains to be explored. Although the Thiele equation can well describe the motion and gyration modes of a skyrmion, the breathing mode information is lost in this equation due to the assumption of non-deformed skyrmion. These questions encourage us to analyse skyrmion dynamics observed in our simulations studies to understand the intrinsic mechanisms.

In this work, we perform a simulation study of a three-terminal racetrack memory device, where a single skyrmion can be written or annihilated via a controller voltage pulse. The effects of the pulse duration and current density on writing and deleting a skyrmion are studied. Based on the results, we are able to revise or correct a train of skyrmion codes by choosing appropriate current pulses. Both gyration and breathing modes are observed during the skyrmions manipulation process. The dynamics of the centre of mass motion for the skyrmion can be described by the Thiele equation derived from the micromagnetic model. We find that the gyrating motion is further modulated due to the coupling to the breathing mode. An analysis of the coupled dynamics was made using a modified Thiele equation that describes well the simulation results.

2   Calculation methods

The model system we use for simulations has parameters appropriate for the Pt (2.7 nm)/$Co_{60}Fe_{20}B_{20}$ (0.8 nm) bilayer (Fig. 1(b)) with the constructed shape shown in Fig. 1(c). The micromagnetic simulations are performed using finite-difference micromagnetic solver MUMAX3 based on the graphic processor unit (GPU).[34] Time-dependent normalized magnetization $\boldsymbol{m} = (m_x, m_y, m_z)$ is governed by the Landau-Lifshitz-Gilbert (LLG) equation which includes the Slonczewski spin-transfer torque (STT),[35]

$$\dot{\boldsymbol{m}} = -\frac{\gamma}{M_S}\boldsymbol{m} \times \left(-\frac{\delta U}{\delta \boldsymbol{m}}\right) + \frac{\gamma \Theta_{SH}\hbar P}{2M_S e d}\{\boldsymbol{m} \times [(\boldsymbol{J}_e \times \boldsymbol{e}_z) \times \boldsymbol{m}]\} + \alpha \boldsymbol{m} \times \dot{\boldsymbol{m}}, \qquad (1)$$

where γ, $\hbar$, e and d are the gyromagnetic ratio, reduced Planck's constant, elementary electronic charge and free layer thickness, respectively. The first term and the third term on the right hand side are field-like torque and damping-like torque, respectively. Here

$$U = U_{ex} + U_{ani} + U_Z + U_{DMI} + U_{demag} = A\int d^2x(\nabla \boldsymbol{m})^2 - K_u\int d^2xm_z^2 - BM_S\int d^2x\, m_z \qquad (2)$$
$$\int d^2x[m_z\text{div}\,\boldsymbol{m} - (\boldsymbol{m}\cdot\nabla)m_z] - \frac{1}{2}M_S\int d^2x\boldsymbol{m}\cdot\boldsymbol{B}_{demag}$$

is the free energy including exchange (U_{ex}), anisotropy (U_{ani}), Zeeman (U_Z), DMI (U_{DMI}), and demagnetizing energy (U_{demag}) terms. The magnetic parameters we adopt for the present simulation study are saturation magnetization $M_S = 1.12 \times 10^6$ A/m, exchange stiffness $A = 10^{-11}$ J/m, perpendicular magnetic anisotropy $K_u = 9.78 \times 10^5$ J/m^3, DMI constant $D = 1.5 \times 10^{-3}$ J/m^2 and Gilbert damping coefficient $\alpha = 0.015$. Values of M_S, A, K_u and D are the same as these were employed in simulations for the Pt/$Co_{60}Fe_{20}B_{20}$ system in a recent work.[9] The Gilbert damping coefficient is extracted from recent experimental studies for ferromagnetic/Pt multilayers.[36] Simulations with different values of α suggests that the damping coefficient does not affect the main results in the present simulation study as discussed later. The demagnetizing field $\boldsymbol{B}_{demag}$ is evaluated as a convolution of the magnetization with a demagnetizing kernel, as described in relevant works in detail.[34] We apply the external field $\boldsymbol{B} = B\boldsymbol{e}_z$ ($B = 15$mT)

antiparallel to the magnetization at a skyrmion core to achieve better skyrmions modification. $\boldsymbol{e}_z$ is the unit vector along z-axis (Fig. 1(c)).

The second term on the right hand side of Eqn (1) is the Slonczewski STT. It is a function of the spin current density J_s with a spin polarization P. The spin current is generated from the charge current $\boldsymbol{J}_e$ applied in the Pt layer due to the spin Hall effect (Fig. 2(b)). Spin Hall angle defined as $\Theta_{SH} = J_s/J_e$ is assumed to be 0.07.[9] $P = 0.4$ is taken into simulations due to the transport of the spin current through the finite heavy metal layer. Charge current distributions in the Pt layer are simulated through a two-dimensional model using the COMSOL multiphysics modelling software, based on which spin-polarized current in the free layer are then also calculated (see Supplementary Note 1). The free layer is discretized into cells of 1 nm × 1 nm × 0.8 nm, with dimensions smaller than the exchange length $l_{ex} = \sqrt{A/\left(\frac{1}{2}\mu_0 M_s^2\right)}$ $= 3.56$ nm to ensure numerical accuracy. Good agreement of the simulated results with recent experimental observations for a similar system [9] leads us to infer the possible realization of our simulations model in future applications.

3   Results and discussion

3.1   Modification of skyrmions information by controller voltage pulses

3.1.1   Current-driven steady motion of skyrmions

The generation of skyrmions has been proposed and demonstrated widely, with either localized spin-polarized current or thermal nucleation.[4, 13, 14] A constricted structure, such as the controller constructed in our simulations, can also be employed to generate skyrmions as shown below. To simplify simulations, we directly write skyrmions at the generator using software packages and then relax them to stable states (Fig. 1(c)). The "1" state is coded by a skyrmion, while a ferromagnetic state is defined as an information "0" (Fig. 1(c)).[19, 21, 31] In a racetrack memory with a generator to write a train of skyrmion codes and a collector to detect them, it is essential to achieve steady motion of skyrmions to keep the spacing constant

between bits. Skyrmions velocity can vary greatly resulting from the competition between SOT and repulsive force from the boundary.[8, 37-39] To minimize the effect, skyrmions are placed at positions with a certain off-centred displacement of the racetrack (Fig. 1(c)), where the force due to spin current and boundary repulsions can be balanced along the y-axis (see Supplementary Fig. 2).[39]
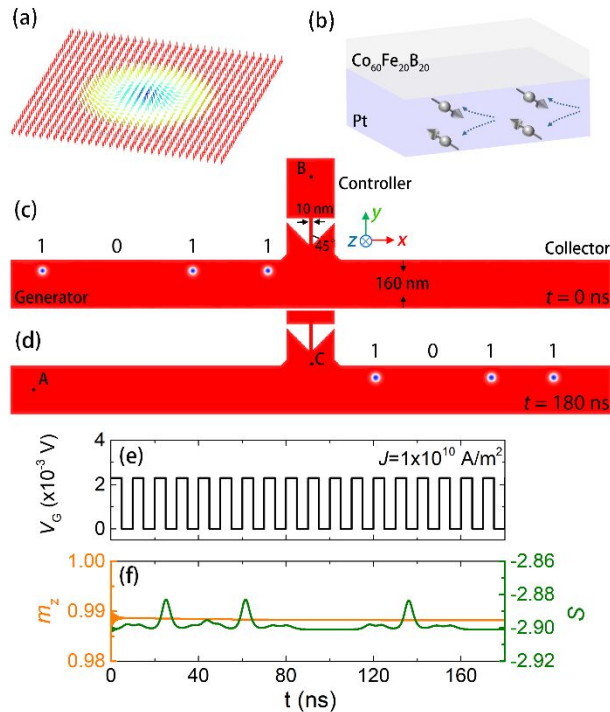

Fig. 1 (a) A Néel-textured skyrmion as favoured in multilayers composed of a ferromagnetic layer and a heavy metal layer with strong spin-orbit coupling. (b) Sketch of $Co_{60}Fe_{20}B_{20}$/Pt bilayers studied in simulations and spin-polarized current generated by spin Hall effect. (c) Schematic of a three-terminal track layout with a generator to write a skyrmion and a collector to detect it. Skyrmion states are proposed to be modified by voltage pulses at the controller. Blue area is with the downward $m_z = -1$ and red area corresponds to the upward $m_z = +1$. Four bits with "1 1 0 1" are placed at the generator with an off-centred displacement along y-axis to compensate for the repulsions of boundary with applied spin-current. Lateral size is marked. (d) Magnetic states at $t = 180$ ns after been driven by voltage pulses. (e) Voltage pulses at the generator which results in charge current $\boldsymbol{J}_e = J\boldsymbol{e}_x$ at the point A. The amplitude of charge current density $J = 1 \times 10^{10}$ A/m^2. $\boldsymbol{e}_x$ is the unit vector along x-axis (insert in (c)). (f) Time-dependent average magnetization m_z and topological number S of the whole pattern.

To drive skyrmions to move toward the collector, we apply voltage pulses at the generator. The electric potential at the collector remains at zero. In this case, the current distributes almost homogeneously along the racetrack (see Supplementary Fig. 1), with the amplitude of $J_e = 1 \times 10^{10}$ A/m^2 (referring to point A in Fig. 1(d)). For this value of J_e, the skyrmions have an average longitudinal velocity of ~ 7.09 m/s that is almost independent on the pulse duration (see Supplementary Note 3). In the absence of any bias voltage at the controller, the skyrmion information is well conserved at the collector (Fig. 1(d), see Supplementary movie 1). The average magnetization m_z and topological number $S = \frac{1}{4\pi}$ $\iint \boldsymbol{m} \cdot (\partial_x \boldsymbol{m} \times \partial_y \boldsymbol{m}) dx dy$ of the whole pattern remain almost unchanged (Fig. 1(f)). S is not an exact integer number because of the boundary spin states and dispersed cells that we use in simulations. Because of the DMI, spin polarizations at the edges are perpendicular to boundaries to minimize the free energy. Three peaks observed in the S pattern correspond to the motion of skyrmions through the controller part where spin structures may vary due to changes of boundary repulsions and SOT. The conserved skyrmion information at the collector can be detected by either using a magnetic tunnel junction or measuring the electronic signal such as Hall resistance.[26]

3.1.2   Generation and annihilation of skyrmions by controller voltage pulses.

To modify a train of skyrmion codes, we first explore the generation and annihilation of an isolated skyrmion via applying a voltage pulse at the controller (V_C). The controller structure proposed in our work involves a narrow channel bordered by 2 surfaces at 45° connection angle to the main track as shown in Fig. 1(c). This geometry is chosen to optimize the modification a train of skyrmion codes. Many works have proposed to write or delete a skyrmion through a narrow track.[21, 40] For example, in processes of conversion, duplication and merging of skyrmions in logic gates, a skyrmion is first converted into a domain-wall pair, and the domain-wall pair is then converted into a skyrmion on the opposite side of the narrow channel.[21] However, the skyrmion generation from a domain-wall pair induces the complexity of the experimental observation, since a domain-wall pair has to be written first, such as, through a magnetic

tunnel junction. We propose in the present simulation study a different process to generate a skyrmion by simply applying controller voltage pulses.

The current along the narrow track depends on the relative potential difference ($\Delta V = V_C - V_{c'}$) between V_C and the voltage at C point ($V_{c'}$) in Fig. 1(d). For positive or negative ΔV, the spin current is along the z-axis but with opposite spin polarization. This allows different ways of skyrmions manipulation. When applying a short and strong V_C pulse ($\Delta V > 0$) with 0.1 ns duration and charge current of $\boldsymbol{J}_e = -J_1 \boldsymbol{e}_y$ (referring to B point in Fig. 1(c), as in subsequent discussions), a reversed domain is nucleated first at the corner of the narrow track (near the C point in Fig. 1(d)) due to the stronger SOT ($t = t_1$ in Fig. 2(a)) while the topological number remains zero. Then the reversed spin texture is driven away by a longer and weaker pulse with τ_g duration and a current of $\boldsymbol{J}_e = -J_2 \boldsymbol{e}_y$ ($t = t_2$ in Fig. 2(a)). After a certain time of τ_g, energetically favorable Bloch line is annihilated and magnetic domain structure transforms into a topological bubble with $S \sim -1$ ($t = t_3$ in Fig. 2(a), and Fig. 2(c)). A single skyrmion corresponding to a minimum in the free energy become stable after switching off the current ($t = t_4$ in Fig. 2(a), see Supplementary movie 2).
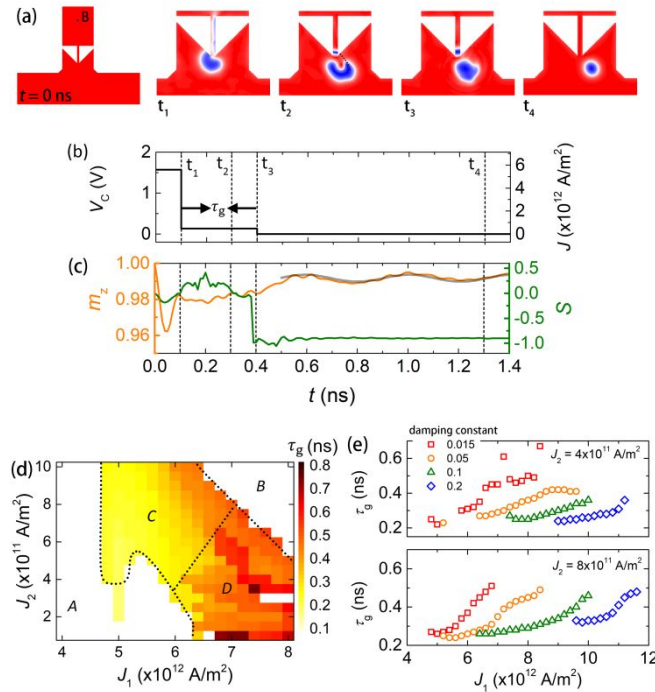
Fig. 2 (a) Top view of magnetic structures at different times $t_1 = 0.1$ ns, $t_2 = 0.3$ ns, $t_3 = 0.4$ ns and $t_4 = 1.3$ ns of the simulation, revealing the nucleation and transformation processes of a single skyrmion. Dotted line at $t = t_2$ is the Bloch line which is stabilized by the spin-orbit torque, and is annihilated at $t = t_3$. (b) A large controller voltage pulse (V_C) with the duration of 0.1 ns ($J_1 = 5 \times 10^{12}$ A/m^2) and a following smaller pulse with the duration of τ_g ($J_2 = 4.6 \times 10^{11}$ A/m^2) are employed to write a skyrmion. Current densities refer to B point at the controller in Fig. 1(c). (c) Average magnetization m_z and topological number S evolutions throughout the skyrmion writing process. The grey line is fitted by a trigonometric function modulated by a damping term. (d) Writing pulse τ_g as functions of charge current densities J_1 and J_2. Skyrmions cannot be written in Phase A and B. Time fluctuation in Phase D results from the competition between current effect and attractive force of boundary for the Bloch domain. (e) The writing pulse duration τ_g of J_2 as a function of the charge current density of J_1 when adopting different values of damping coefficients.

The pulse width τ_g needed to generate a skyrmion depends greatly on J_1 and J_2, as presented in Fig. 2(d). At comparatively low amplitudes of current density (Phase A in Fig. 2(d)), reversed spin texture cannot be driven away from the boundary (see Supplementary movie 3). When applying both large J_1 and J_2 (Phase B in Fig. 2(d)), the magnetic bubble will touch the edge of racetrack before a skyrmion is transformed with annihilation of the Bloch point. This is because the textured area increases greatly with a large SOT (see

Supplementary movie 4). In both cases, skyrmions cannot be written. Only when current is in a certain range (Phases C and D in Fig. 2(d)), can a skyrmion be converted from a magnetic domain. In Phase C, τ_g unusually increases with a large current density. It is attributed to energetically favourable Bloch line stabilized by SOT.[9] An irregular relationship of τ_g with current density has been observed in Phase D, because an intermediate state, skyrmionium, is transformed before converting into a stable skyrmion (see Supplementary movie 5). Based on these results, we can choose an appropriate composite of current pulses to generate a single skyrmion.

Underlying mechanisms for skyrmion generation may be different, depending on magnetic parameters of an independent system. In a multilayer with a smaller value of DMI constant, skyrmions are formed by conversions of a chiral domain wall or a turbulent magnetization texture,[25] while the skyrmion with a smaller skyrmion size is transformed from a magnetic bubble with the topological number of zero in our simulations. However, a constricted structure is still one of the most effective ways to generate a skyrmion in a real sample, because of the convenience of both fabrication and operation in experiments.[9, 41]

The skyrmion generation has also been realized in simulations adopting different values of the damping coefficient ($\alpha = 0.015, 0.05, 0.1$ and 0.2). The current densities required to generate a skyrmion increase with increasing damping coefficient, as presented in Fig. 2(e), because of the slower precession of magnetization. However, the qualitative features of the skyrmion generation process remain the same for different values of the damping coefficient. This confirms the robustness of the proposed configuration to write a skyrmion. One can decrease the current density to generate a skyrmion by increasing the pulse duration, similar as experimental observations of nucleation of a skyrmion through a defect.[9] The current density can also be further decreased by manipulating current pulse shape. This is suggested by a recent study that it is much easier to generate a skyrmion through a defect by employing a bipolar current pulse than by employing a composed current pulse similar as the current pulses we use to generate a skyrmion.[27]
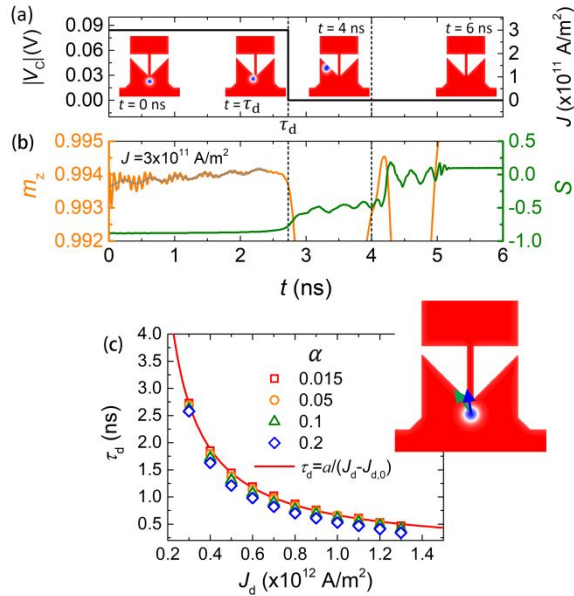
Fig. 3 (a) A negative controller voltage pulse ($\tau_d = 2.73$ ns, $J_e = J_d e_y$ referring to B point in Fig. 1(c) with $J_d = 3 \times 10^{11}$ A/m^2) applied to delete a skyrmion. Inserts are top view of spin structures at different simulated times. (b) Average magnetization m_z and topological number S evolutions during skyrmion annihilation. The grey line is fitted by a trigonometric function modulated by a damping term. (c) τ_d as a function of charge current density J_d employed with adopting different values of the damping coefficient. Solid line is fitted by $\tau_d = \frac{a}{(J_d - J_{d,0})}$ with fitted $a = 620$ A · s/ m^2, and $J_{d,0} = 0.073 \times 10^{12}$ A/m^2 for the damping coefficient $\alpha = 0.015$.

When we apply a negative V_C pulse ($\Delta V < 0$) with the duration τ_d, a skyrmion can be driven toward the boundary and then annihilated (Fig. 3(a), see Supplementary movie 6). The time τ_d required to delete a skyrmion decreases with increasing current density J_d and eventually saturates. The function of τ_d versus J_d is well described by the formula $\tau_d = \frac{a}{(J_d - J_{d,0})}$, as suggested from a macro-spin model,[42, 43] which is illustrated in Fig. 3(c). Here a relates to an effective charge parameter that represents the number of electrons required to delete a skyrmion. There is a critical charge current $J_{d,0}$ to strike out a skyrmion, due to boundary repulsion. The inverse relationship can also be approximately understood from the aspect of skyrmion motion. Because of the finite distance l_{s-e} from the initial position of a skyrmion to the racetrack boundary, the time required to drive a skyrmion to the boundary is inverse proportional to its velocity and

therefore to the current density.[44] Spin texture vibrates after touching the boundary until it disappears completely. The vibration, together with two plateaus observed in $S(t)$ ($t > 2.73$ ns in Fig. 3(b)), is attributed to disparity of spin configurations during the skyrmion annihilation (see Supplementary movie 6).

In contrast to the dependence of current densities on α when generating a skyrmion, the pulse duration τ_d as a function of the charge current density of J_d to delete a skyrmion is almost independent of the damping coefficient (Fig. 3(c)). It has been revealed that the skyrmion velocity decreases with increasing the damping constant.[38] On the other hand, an increase in α changes skyrmion trajectory thus decreases the value of l_{s-e} (the insert in Fig. 3(c)). Competition between the two factors result in negligible dependence of τ_d on the damping coefficient.

3.1.3   Modification of a train of skyrmion codes in a controlled manner.

We can integrate the processes of writing and deleting a single skyrmion to explore the modification of a train of skyrmion codes in a controlled manner. In the work by D. Zhu, et al,[24] a four-terminal racetrack device was proposed for manipulating the signal carried by a train of skyrmions. In this scheme, the driving current for the skyrmion is first switched off, then the writing or deletion of a skyrmion is accomplished by applying a current through two narrow tracks terminals on both sides of the main track.[24] By comparison, the proposed racetrack device in our studies has one less terminal and involves a simple generation or deletion procedure for a skyrmion at the controller. This is important from both the fabrication and application points of view. It features less energy consumption as well as storage space reduction. Moreover, due to the additional space between the controller and the main track, the driving current has only a small effect on skyrmion motion at the controller part in our setup. Thus it is expected to modify the skyrmion information without switching off the driving current pulses. This leads to the reduced complexity of the device operation. We show below that the skyrmion information can be modified in a controlled manner in our proposed configuration.

An initial state coded with "1 1 0 1" is presented in Fig. 4(a). Skyrmions are driven by voltage

pulses at the generator and move along the magnetic nanoribbon as illustrated in Fig. 1. We apply a negative

V_C pulse with $\tau_d = 0.1$ ns and $J_d = 2 \times 10^{12}$ A/m^2 (referring to B point in Fig. 1(c)) to annihilate the second

skyrmion when it approaches the controller ($t = 61.6$ ns). The second bit of "1" then transforms into "0",

and the code "1 0 0 1" keeps moving. After a duration of time, a new skyrmion is generated by a composite

voltage pulse at the controller ($t = 99.7$ ns). This changes the third bit "0" into "1". The final state with the

information "1 0 1 1" is collected at the collector with almost conserved spacing between two bits (Fig.

4(b)). Thus, the controlled modification of a train of skyrmions information is realized (see Supplementary

movie 7). During the process, the topological number varies from -3 to -2, and back to -3, corresponding to

the annihilation and generation of a skyrmion. The other circumstance of transforming "1 1 0 1" to "1 0 1

1" have also been tested to ensure the validity of the proposed method (see Supplementary movie 8). Similar

to the racetrack memory based on magnetic domain walls,[45] the revised skyrmion information can be stored

in a long racetrack where multiple controller and collector terminals can be present. To modify spin states

in a controlled manner, it is crucial to detect the skyrmion code at the controller. It has been proposed to

realize this via tunnelling magnetoresistance,[46] while the "0" state can be visualized by a correlated
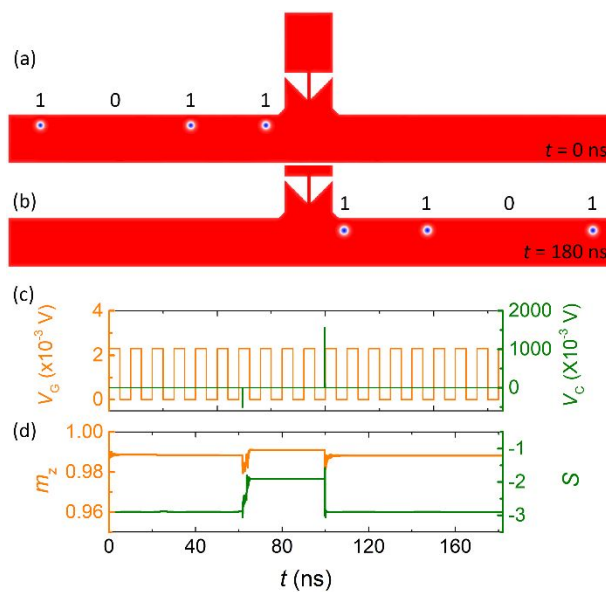
structure.[47]

Fig. 4 (a) The initial magnetic state with the code of "1 1 0 1" is placed at the generator at $t = 0$ ns. (b) The revised information of "1 0 1 1" collected at the collector at $t = 180$ ns. (c) A train of voltage pulses are exerted at the generator (V_G) ($J = 1 \times 10^{10}$ A/m^2 referring to A point in Fig. 1(d)) to drive skyrmions to move along the racetrack memory. At $t = 61.6$ ns, a negative V_C pulse ($\tau_d = 0.1$ ns, $J_d = 2 \times 10^{12}$ A/m^2) is applied to delete a skyrmion. At $t = 99.7$ ns, a composite positive V_C pulse ($J_1 = 5 \times 10^{12}$ A/m^2 with the duration of 0.1 ns and a following current $J_2 = 4 \times 10^{11}$ A/m^2 with $\tau_g = 0.28$ ns) is applied to write a skyrmion. (d) Average magnetization m_z and topological number S evolutions along controllably modifying skyrmions information.

In Fig. 4(b), it can be seen that although the modified information can be obviously identified, the distance between two skyrmions changes slightly compared with the initial state (Fig. 4(a)). Similar phenomenon has also been observed in Fig. 1(d). This results from the Magnus force ($\boldsymbol{G} \times \dot{\boldsymbol{r}}$ in Eqn (3)) with a non-zero y-component, known as the skyrmion Hall effect.[10, 28, 48] In the process of transporting a skyrmion, transverse motion of a skyrmion can be avoided by cancelling out Magnus force with boundary repulsions. However, skyrmion Hall effect is fatal when generating or annihilating a skyrmion with the large current applied. In addition to the skyrmion motion, skyrmion size also depends on the current. To generate a skyrmion, a large current pulse with longer duration is applied, giving rise to increasing radii of other skyrmions (see Supplementary movie 7). Thus it is essential to apply an out-of-plane magnetic field $B = 15$ mT to maintain skyrmions information. In the absence of this additional magnetic field, the radius of a spin texture would increase greatly and then touch the boundary. Otherwise if we apply a large external field, the generation of a new skyrmion at the controller is prevented. Both the applied magnetic field and appropriate current pulses ensure the manipulation of skyrmions in a controlled manner. Controlled modification of a skyrmion with no external field applied remains to be explored.

3.2   Coupling between gyration and breathing modes of skyrmions observed during skyrmion manipulation in the device.

Interestingly, we observe time dependent magnetic oscillations of the magnetization m_z during both skyrmions writing (Fig. 2(c)) and deletion (Fig. 3(b)) processes. Two oscillation modes with frequencies ν_1

~ 2.4 GHz and $\nu_2 \sim 10$ GHz are identified. The mode with a large frequency ν_2 results from the oscillation of the magnetization at the racetrack boundary, and it disappears when the boundary spin states are not included (Fig. 5(a)). Frequency ν_1 corresponds to the breathing mode of a skyrmion. This is confirmed via a direct study of the oscillatory variation of the skyrmion radius as illustrated in Fig. 5(a). Besides the breathing mode, we have also observed an oscillatory time dependence in the trajectories of the skyrmion centre of mass during skyrmions manipulation (Fig. 5(b)), corresponding to a gyration mode.[49]
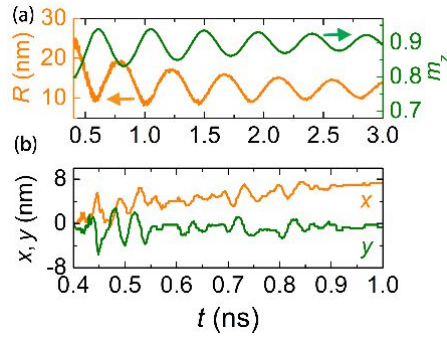

Fig. 5 (a) Time-dependent average magnetization m_z (green) and the radius R (orange) for a skyrmion after being generated in the three-terminal racetrack memory. (b) The time variation of relative coordinates (x, y) of the centre of mass of the skyrmion centre of mass after it is generated at the time $t = 0.4$ ns, as illustrated in Fig. 2.

We can understand the gyration mode of a skyrmion approximately via the Thiele equation derived from the LLG equation. However, a non-deformed skyrmion is assumed in the derivation of this equation.[50, 51] We employ the Thiele equation here in a more phenomenological fashion by allowing a time dependence in the radius of the skyrmion as well as taking the inertial mass and Slonczewski SOT into consideration. A modified Thiele equation results as in Eqn (3)

$$\frac{\gamma}{M_S d} M \ddot{\boldsymbol{r}} + \boldsymbol{G} \times \dot{\boldsymbol{r}} + \alpha \mathcal{D} \dot{\boldsymbol{r}} + \mathcal{T} R \overleftrightarrow{\boldsymbol{\Gamma}} (\boldsymbol{J}_e \times \boldsymbol{e}_z) - \frac{\gamma}{M_S d} \boldsymbol{F} = 0. \tag{3}$$

Here M is the effective inertial mass of a skyrmion, which has been demonstrated to be crucial in describing gigahertz gyro trajectories observed in magnetic disks;[5, 29, 52, 53] $\ddot{\boldsymbol{r}}$ is the accelerating rate of the spin texture. The second term and the third term are known as Magnus force and dissipative force,

respectively. $\boldsymbol{G} = \mathcal{G}\boldsymbol{e}_z$ is the gyro coupling vector with $\mathcal{G} = 4\pi S$, where S is the topological number of a skyrmion, which is -1 in our simulations. $\mathcal{D} \approx 19.3373$ is the dissipation parameter. The fourth term is integrated from Slonczewski STT shown in Eqn (1). It is a function of the skyrmion radius R with the tensor

$$\overleftrightarrow{\Gamma} = \begin{bmatrix} 0 & -1 & 0 \\ 1 & 0 & 0 \\ 0 & 0 & 0 \end{bmatrix} \text{ and } \mathcal{T} = \frac{\gamma\Theta_{SH}\hbar P\pi^2}{2M_s e d\ 2}. \quad \boldsymbol{F} = -\partial_r U \text{ is the repulsive force from the racetrack boundary as a}$$

spatial derivation of U exactly described in Eqn (2). Generally, $\boldsymbol{F} = -\partial_r U = -K\boldsymbol{r}$ is suggested in most studies and explains well the skyrmion dynamics observed in experiments.[5, 15, 54] It is reasonable when a skyrmion is confined in a small region. Recent studies show that K actually is a variable value depending on the off-centred displacement.[44] In our simulations, we take a first-order expansion of the boundary force when the skyrmion is around the position $\boldsymbol{r} = \boldsymbol{r}_0$. This gives $\boldsymbol{F}(\boldsymbol{r}) = \boldsymbol{F}(\boldsymbol{r}_0) + \overleftrightarrow{K}(\boldsymbol{r} - \boldsymbol{r}_0)$. The redefined $\overleftrightarrow{K}$

$$= \partial_r \boldsymbol{F} = \begin{bmatrix} \mathcal{K}_{xx} & \mathcal{K}_{xy} & 0 \\ \mathcal{K}_{yx} & \mathcal{K}_{yy} & 0 \\ 0 & 0 & 0 \end{bmatrix} \text{ can be directly derived from the micromagnetic simulations. For a skyrmion in a}$$

racetrack, $\mathcal{K}_{yy} = \mathcal{K}$ has a finite value while others remain zero. In our simulations, we simplify $\overleftrightarrow{K}$ to be a scalar value $\mathcal{K}$ which is only a function of the distance from the skyrmion centre of mass to the racetrack boundary (see Supplementary Note 5). Unlike the original Thiele equation with a fixed radius R for the skyrmion, here the time dependence of the radius $R(t)$ has to be treated as an input for determining how the center of mass trajectory $\boldsymbol{r}(t)$ is coupled to the breathing mode dynamics.

During the skyrmions manipulation, both the trajectory of the skyrmion core ($\boldsymbol{r}(t)$) and the variation of the skyrmion radius ($R(t)$) can be decomposed into a slow time varying part ($\boldsymbol{r}_0(t)$ and $R_0(t)$) and a more rapidly oscillatory time dependent part. We perform a fast Fourier transformation (FFT) for the oscillatory parts yielding

$$\boldsymbol{r}(t) = \boldsymbol{r}_0(t) + \Delta x \boldsymbol{e}_x + \Delta y \boldsymbol{e}_y = \boldsymbol{r}_0(t) + \sum_{i=x,y} \int_{0^+}^{+\infty} dv \left[A_i'(v)\cos 2\pi v t - A_i''(v)\sin 2\pi v t \right] \boldsymbol{e}_i \tag{4}$$

$$R(t) = R_0(t) + \int_{0^+}^{+\infty} dv \left[\Delta R'(v)\cos 2\pi v t - \Delta R''(v)\sin 2\pi v t \right]. \tag{5}$$

16

For the gyrating motion of a skyrmion, $\frac{\pi}{2}$-phase difference between x- and y-components of the oscillation

has been observed (Fig. 5(b)). This indicates $A'_x = -A''_y$ and $A''_x = A'_y$, if we assume the amplitude of $\left|A_x(v)\right|$

$= \left|A'_x(v) + iA''_x(v)\right|$ is the same as $\left|A_y(v)\right| = \left|A'_y(v) + iA''_y(v)\right|$. Substituting Eqns. (4) and (5) into the Eqn

(3), and proceeding as detailed in Supplementary Note 4, leads to the result

$$A_x(v) = \chi(v, J_e, K)\Delta R(v), \, A_y(v) = -iA_x(v) \tag{6}$$

where

$$\chi(v, J_e, K) = \cfrac{\frac{1}{2}\mathcal{T}J_e}{-\frac{\gamma}{M_s d}M(2\pi)^2 v^2 + 2\pi(-\mathcal{G} + i\alpha\mathcal{D})v + \frac{\gamma}{2M_s d}\mathcal{K}} \tag{7}$$

is basically the response function describing how the gyrating motion of the centre of mass described by (A_i

$(v) = A'_i(v) + iA''_i(v)$ ($i = x$ or y)) responds to the breathing mode dynamics described by $\Delta R(v) = \Delta R'(v)$

$+ i\Delta R''(v)$. The breathing mode spectrum can be derived from the micromagnetic simulations, as presented

in Fig. 6. We assume the mass density $\rho = 2.07 \times 10^{-8}$ kg/m^2 of a skyrmion in our studies a constant (see

Supplementary Note 6 and 7). The inertial mass is determined to be $M = 2\pi\rho Rd = 1.135 \times 10^{-24}$ kg with

the radius $R = 10.95$ nm. We consider here the details of the gyration and breathing mode dynamics during

the skyrmion annihilation process. The main peak in the Fourier spectrum of the gyration mode spectrum

found from the micromagnetic simulations at about 8.5 GHz is well reproduced through the function

$\left|A_i(v)\right|$ ($i = x$ or y) given by Eqn (6) (Fig. 6). Also, due to the coupling of the gyration and breathing mode,

there is a weaker peak in the frequency spectrum of the gyration mode from the simulation studies at about

2.4 GHz. This feature is also present in the analytic result from Eqn (6) (Fig. 6). Thus, the main features of

the observed gyration mode dynamics in the micromagnetic simulation studies are well understood from

the coupling of the breathing mode and the gyration mode from the Thiele equation as shown in Eqn (3).

We note that the gyrating motion of a skyrmion after being generated (Fig. 5(b)) in the writing process is

quite different from that observed during the skyrmion annihilation process, since the skyrmion has a larger size and an irregular shape of the spin texture right after the generation process (Fig. 2).
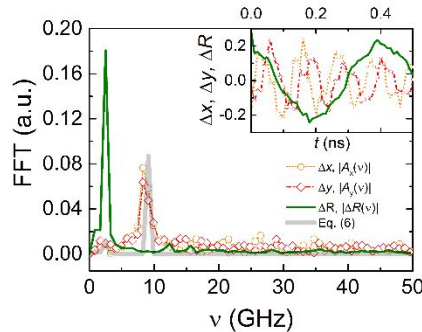

Fig. 6 The FFT spectra ($|\Delta R(\nu)|$, $|A_x(\nu)|$, and $|A_y(\nu)|$, respectively) of the breathing mode (ΔR) for a skyrmion, and trajectories of the centre of mass (Δx and Δy) observed during skyrmions annihilation process with the current J_d $= 3 \times 10^{11} \, \text{A/m}^2$ applied. Grey line is calculated from Eqns. (6) and (7) with the mass $M = 1.135 \times 10^{-24} \, \text{kg}$ and the stiffness $\mathcal{K} = 1 \times 10^{-4} \, \text{N/m}$ adopted. It is presented with five times magnification. The stiffness $\mathcal{K}$ is inferred from the distance (24.46 nm) from the skyrmion centre of mass to the racetrack edge (see Supplementary Note 5). Insert curves represent the real-time spectra of breathing and gyration modes for a skyrmion observed during skyrmions annihilation process. In the simulation, we take a small cell of $0.25 \, \text{nm} \times 0.25 \, \text{nm} \times 0.8 \, \text{nm}$ to define the position of the skyrmion core.

Although the inertia mass required to understand the dynamics of the skyrmion from the micromagnetic simulations is one order of magnitude smaller than the mass observed in recent experiments and simulations, the mass density shows the same magnitude with that reported,[5, 29, 52] due to the small skyrmion radius in our studies. The skyrmion size is determined by magnetic parameters employed, especially the out-of-plane magnetic field. We note here that the mass density is a more meaningful parameter compared with the inertial mass when studying the skyrmion dynamics (see Supplementary Note 7). The inertial mass density of a skyrmion is much larger than that reported for straight domain walls and the difference has been attributed to the local topological spin structure.[55, 56]

3.3 Discussions on experimental feasibility of the proposed configuration

The skyrmion size in our simulations is much smaller than experimental observations in similar systems.[8, 9] This is because of the application of a perpendicular field and larger K_u and D adopted in simulations.[57-59] It has been theoretically shown that both decreases in K_u and D/A would lead to the increases in skyrmion radius.[60, 61] A skyrmion with a large size may have a larger skyrmion velocity and a smaller skyrmion Hall angle.[10] The increases in skyrmion velocity may improve the efficiency of the performance of the proposed memory. However, the device size would also increase to modify skyrmion information. The changes in skyrmion Hall angle may have little effect on skyrmion motion in the racetrack memory, because of the balance between the Magnus force and repulsive force from boundaries.

In our simulations, we delete a skyrmion by driving the skyrmion to the racetrack boundary. It has been theoretically shown that the critical boundary force to overcome when deleting a skyrmion linearly increases with increasing $D_0 = D/\sqrt{A\left(K_u - \mu_0 M_s^2/2\right)}$. This infers that the critical current density to strike out a skyrmion may decrease with decreasing D_0. Using a narrow track to generate a skyrmion is robust as many experimental observations and simulation studies.[9, 25] In our simulations, we provide an effective method to modify a train of skyrmion codes, which can be realized in experiments as discussed following.

Although the present studies are performed using zero-temperature micromagnetic simulations, the proposal of using a three-terminal racetrack device to modify skyrmions information is feasible in experiments from both device fabrication and operation aspects. Well-developed lithography experiments provide effective methods to fabricate the proposed device, and also Cr/Au patterns to achieve electrical contacts with external sources. Even though skyrmions manipulation occurs on the nanosecond time scale, skyrmions are static in a real sample when the current pulse is switched off and can therefore be detected by static measurements.[9, 48] A finite temperature may have an influence on the device operation. However, the thermal fluctuation promotes magnetization switching, essential for skyrmion nucleation or deletion, with a lower current density. This is desirable for skyrmion-based applications with lower-energy consumption.[9]

In experimental studies, multiple layer repetitions are grown in order to enhance magnetic contrast in the X-ray magnetic circular dichroism signal or the Lorentz transmission electron microscopy signal. The repetitions of the multilayer may have an influence on magnetic parameters of the system and also the stray field. Nevertheless, it has been shown that with proper choice of the parameters in the micromagnetic model, zero-temperature simulations with only one unit cell in the z-direction well reproduce experimental results observed in multiple layer repetitions.[9] This leads us to believe that the proposed structure here can be realized in actual experiments.

Finally, recent experiments have observed gyration modes of a skyrmion with an influence on the skyrmions motion.[5] From a fundamental physics point of view, understanding the dynamics of skyrmions is of great interest. It is also of great significance to help understand and design skyrmions manipulation in future experimental studies.

4   Conclusions

In summary, we have constructed a three-terminal racetrack memory, where magnetic information coded with "1" and "0" via presence or absence of a skyrmion can be converted into each other by voltage pulses at the controller. The effects of current density and pulse duration on skyrmions generation and annihilation are discussed. The skyrmion generation starts from the nucleation of a reversed domain wall. This is different from the process of skyrmion generation from a domain-wall pair as reported in many previous works.[21, 40] We have shown that a train of skyrmion codes can be modified in a controlled manner. In the proposed configuration, skyrmion information can be modified without switching off the driving current pulses. In addition, the device proposed in this study involves one less terminal compared to a previous proposal[24] and it features less energy consumption as well as storage space reduction, leading to reduced complexity of the device operation. We have also employed a modified Thiele equation to analyse the coupled gyration and breathing modes observed during skyrmions manipulation. At present, to achieve steady motion of skyrmions while keeping information undistorted in complex structures remains a

fundamental challenge due to the unavoidable Magnus force. Our results provide a simple method of gate-controlled modification of a train of skyrmion codes in a racetrack memory, which is different from previous proposals of logic gates that are realized in Y-junction channels. Deep insight into the physics of inertial mass and breathing modes is crucial to understanding the skyrmions manipulation. It paves the way for development of advanced skyrmion-based spintronic applications.

Conflicts of interest

There are no conflicts to declare.

Acknowledgements

References

1.   X. Yu, Y. Onose, N. Kanazawa, J. Park, J. Han, Y. Matsui, N. Nagaosa and Y. Tokura, *Nature*, 2010, **465**, 901.
2.   X. Yu, N. Kanazawa, Y. Onose, K. Kimoto, W. Zhang, S. Ishiwata, Y. Matsui and Y. Tokura, *Nat. Mater.*, 2011, **10**, 106.
3.   N. Nagaosa and Y. Tokura, *Nat. Nanotech.*, 2013, **8**, 899.
4.   N. Romming, C. Hanneken, M. Menzel, J. E. Bickel, B. Wolter, K. von Bergmann, A. Kubetzka and R. Wiesendanger, *Science*, 2013, **341**, 636-639.
5.   F. Büttner, C. Moutafis, M. Schneider, B. Krüger, C. Günther, J. Geilhufe, C. v. K. Schmising, J. Mohanty, B. Pfau and S. Schaffert, *Nat. Phys.*, 2015, **11**, 225.
6.   W. Jiang, P. Upadhyaya, W. Zhang, G. Yu, M. B. Jungfleisch, F. Y. Fradin, J. E. Pearson, Y. Tserkovnyak, K. L. Wang and O. Heinonen, *Science*, 2015, **349**, 283-286.
7.   C. Moreau-Luchaire, C. Moutafis, N. Reyren, J. Sampaio, C. Vaz, N. Van Horne, K. Bouzehouane, K. Garcia, C. Deranlot and P. Warnicke, *Nat. Nanotech.*, 2016, **11**, 444.
8.   S. Woo, K. Litzius, B. Krüger, M.-Y. Im, L. Caretta, K. Richter, M. Mann, A. Krone, R. M. Reeve and M. Weigand, *Nat. Mater.*, 2016, **15**, 501.
9.   F. Büttner, I. Lemesh, M. Schneider, B. Pfau, C. M. Günther, P. Hessing, J. Geilhufe, L. Caretta, D. Engel and B. Krüger, *Nat. Nanotech.*, 2017, **12**, 1040.
10.   K. Litzius, I. Lemesh, B. Krüger, P. Bassirian, L. Caretta, K. Richter, F. Büttner, K. Sato, O. A. Tretiakov and J. Förster, *Nat. Phys.*, 2017, **13**, 170.
11.   A. Nych, J.-i. Fukuda, U. Ognysta, S. Žumer and I. Muševič, *Nat. Phys.*, 2017, **13**, 1215.

12.   A. Soumyanarayanan, M. Raju, A. G. Oyarce, A. K. Tan, M.-Y. Im, A. P. Petrović, P. Ho, K. Khoo, M. Tran and C. Gan, *Nat. Mater.*, 2017, **16**, 898.
13.   J. Sampaio, V. Cros, S. Rohart, A. Thiaville and A. Fert, *Nat. Nanotech.*, 2013, **8**, 839.
14.   W. Legrand, D. Maccariello, N. Reyren, K. Garcia, C. Moutafis, C. Moreau-Luchaire, S. Collin, K. Bouzehouane, V. Cros and A. Fert, *Nano Lett.*, 2017, **17**, 2703-2712.
15.   X. Wang, W. Gan, J. Martinez, F. Tan, M. Jalil and W. Lew, *Nanoscale*, 2018, **10**, 733-740.
16.   S. D. Pollard, J. A. Garlow, J. Yu, Z. Wang, Y. Zhu and H. Yang, *Nat. Commun.*, 2017, **8**, 14761.
17.   M. Schott, A. Bernand-Mantel, L. Ranno, S. Pizzini, J. Vogel, H. Bea, C. Baraduc, S. Auffret, G. Gaudin and D. Givord, *Nano Lett.*, 2017, **17**, 3006-3012.
18.   R. Wiesendanger, *Nat. Rev. Mater.*, 2016, **1**, 16044.
19.   A. Fert, V. Cros and J. Sampaio, *Nat. Nanotech.*, 2013, **8**, 152.
20.   D. Prychynenko, M. Sitte, K. Litzius, B. Krüger, G. Bourianoff, M. Kläui, J. Sinova and K. Everschor-Sitte, *Phys. Rev. Appl.*, 2018, **9**, 014034.
21.   X. Zhang, M. Ezawa and Y. Zhou, *Sci. Rep.*, 2015, **5**, 9400.
22.   G. Yu, P. Upadhyaya, Q. Shao, H. Wu, G. Yin, X. Li, C. He, W. Jiang, X. Han and P. K. Amiri, *Nano Lett.*, 2016, **17**, 261-268.
23.   S. Luo, M. Song, X. Li, Y. Zhang, J. Hong, X. Yang, X. Zou, N. Xu and L. You, *Nano Lett.*, 2018, **18**, 1180-1184.
24.   D. Zhu, W. Kang, S. Li, Y. Huang, X. Zhang, Y. Zhou and W. Zhao, *IEEE Trans. Electron Devices*, 2018, **65**, 87-95.
25.   O. Heinonen, W. Jiang, H. Somaily, S. G. Te Velthuis and A. Hoffmann, *Phys. Rev. B*, 2016, **93**, 094407.
26.   D. Maccariello, W. Legrand, N. Reyren, K. Garcia, K. Bouzehouane, S. Collin, V. Cros and A. Fert, *Nat. Nanotech.*, 2018, **13**, 233.
27.   S. Woo, K. M. Song, X. Zhang, M. Ezawa, Y. Zhou, X. Liu, M. Weigand, S. Finizio, J. Raabe and M.-C. Park, *Nat. Electron.*, 2018, **1**, 288.
28.   P. Dürrenfeld, Y. Xu, J. Åkerman and Y. Zhou, *Phys. Rev. B*, 2017, **96**, 054430.
29.   I. Makhfudz, B. Krüger and O. Tchernyshyov, *Phys. Rev. Lett.*, 2012, **109**, 217201.
30.   J.-V. Kim, F. Garcia-Sanchez, J. Sampaio, C. Moreau-Luchaire, V. Cros and A. Fert, *Phys. Rev. B*, 2014, **90**, 064410.
31.   R. Tomasello, E. Martinez, R. Zivieri, L. Torres, M. Carpentieri and G. Finocchio, *Sci. Rep.*, 2014, **4**, 6784.
32.   Y. Zhou, E. Iacocca, A. A. Awad, R. K. Dumas, F. Zhang, H. B. Braun and J. Åkerman, *Nat. Commun.*, 2015, **6**, 8193.
33.   J. Kim, J. Yang, Y.-J. Cho, B. Kim and S.-K. Kim, *J. Appl. Phys.*, 2018, **123**, 053903.
34.   A. Vansteenkiste, J. Leliaert, M. Dvornik, M. Helsen, F. Garcia-Sanchez and B. Van Waeyenberge, *AIP Adv.*, 2014, **4**, 107133.
35.   J. C. Slonczewski, *J. Magn. Magn. Mater.*, 1996, **159**, L1-L7.
36.   S. Iihama, S. Mizukami, H. Naganuma, M. Oogane, Y. Ando and T. Miyazaki, *Phys. Rev. B*, 2014, **89**, 174416.
37.   J. Iwasaki, M. Mochizuki and N. Nagaosa, *Nat. Nanotech.*, 2013, **8**, 742.
38.   J. Iwasaki, W. Koshibae and N. Nagaosa, *Nano Lett.*, 2014, **14**, 4432-4437.
39.   Y. Zhang, S. Luo, B. Yan, J. Ou-Yang, X. Yang, S. Chen, B. Zhu and L. You, *Nanoscale*, 2017, **9**, 10212-10218.
40.   Y. Zhou and M. Ezawa, *Nat. Commun.*, 2014, **5**, 4652.
41.   A. Hrabec, J. Sampaio, M. Belmeguenai, I. Gross, R. Weil, S. M. Chérif, A. Stashkevich, V. Jacques, A. Thiaville and S. Rohart, *Nat. Commun.*, 2017, **8**, 15765.

42.   K. Garello, C. O. Avci, I. M. Miron, M. Baumgartner, A. Ghosh, S. Auffret, O. Boulle, G. Gaudin and P. Gambardella, *Appl. Phys. Lett.*, 2014, **105**, 212402.

43.   H. Liu, D. Bedau, J. Sun, S. Mangin, E. Fullerton, J. Katine and A. Kent, *J. Magn. Magn. Mater.*, 2014, **358**, 233-258.

44.   M.-W. Yoo, V. Cros and J.-V. Kim, *Phys. Rev. B*, 2017, **95**, 184423.

45.   S. S. Parkin, M. Hayashi and L. Thomas, *Science*, 2008, **320**, 190-194.

46.   C. Hanneken, F. Otte, A. Kubetzka, B. Dupé, N. Romming, K. Von Bergmann, R. Wiesendanger and S. Heinze, *Nat. Nanotech.*, 2015, **10**, 1039.

47.   W. Kang, C. Zheng, Y. Huang, X. Zhang, Y. Zhou, W. Lv and W. Zhao, *IEEE Electron Device Lett.*, 2016, **37**, 924-927.

48.   W. Jiang, X. Zhang, G. Yu, W. Zhang, X. Wang, M. B. Jungfleisch, J. E. Pearson, X. Cheng, O. Heinonen and K. L. Wang, *Nat. Phys.*, 2017, **13**, 162.

49.   J. Kim, J. Yang, Y.-J. Cho, B. Kim and S.-K. Kim, *Sci. Rep.*, 2017, **7**, 45185.

50.   A. Thiele, *Phys. Rev. Lett.*, 1973, **30**, 230.

51.   S. Seki and M. Mochizuki, in *Skyrmions in Magnetic Materials*, Springer, 2016, pp. 33-56.

52.   T. Shiino, K.-J. Kim, K.-S. Lee and B.-G. Park, *Sci. Rep.*, 2017, **7**, 13993.

53.   V. P. Kravchuk, D. D. Sheka, U. K. Rößler, J. van den Brink and Y. Gaididei, *Phys. Rev. B*, 2018, **97**, 064403.

54.   J. Martinez and M. Jalil, *J. Magn. Magn. Mater.*, 2017, **424**, 291-297.

55.   D. Bedau, M. Kläui, S. Krzyk, U. Rüdiger, G. Faini and L. Vila, *Phys. Rev. Lett.*, 2007, **99**, 146601.

56.   J. Vogel, M. Bonfim, N. Rougemaille, O. Boulle, I. M. Miron, S. Auffret, B. Rodmacq, G. Gaudin, J. Cezar and F. Sirotti, *Phys. Rev. Lett.*, 2012, **108**, 247202.

57.   S. Woo, K. M. Song, H.-S. Han, M.-S. Jung, M.-Y. Im, K.-S. Lee, K. S. Song, P. Fischer, J.-I. Hong and J. W. Choi, *Nat. Commun.*, 2017, **8**, 15573.

58.   K. Di, V. L. Zhang, H. S. Lim, S. C. Ng, M. H. Kuok, X. Qiu and H. Yang, *Appl. Phys. Lett.*, 2015, **106**, 052403.

59.   S. Tacchi, R. Troncoso, M. Ahlberg, G. Gubbiotti, M. Madami, J. Åkerman and P. Landeros, *Phys. Rev. Lett.*, 2017, **118**, 147201.

60.   X. Zhang, G. Zhao, H. Fangohr, J. P. Liu, W. Xia, J. Xia and F. Morvan, *Sci. Rep.*, 2015, **5**, 7643.

61.   A. Siemens, Y. Zhang, J. Hagemeister, E. Vedmedenko and R. Wiesendanger, *New Journal of Physics*, 2016, **18**, 045021.

A table of content entry

We propose in a racetrack memory to modify skyrmion information, and study the coupling between two oscillatory modes of skyrmions.